Supplementary Information

Alkaline silver nitrate exhibits versatility in the instant oxidation of furans to bioplastic precursors and its mechanistic insights

Ravi Kumar Kunchala,[1, †] Meera Cheviri,[1, †] Paramdeep Kaur,[1] Bhawana Devi[1], Lakshmanan Potturaja,[1] Vishnu Bakthavachalam,[1] Senthil Murugan Arumugam,[1] Alisha Alisha,[1,2] Jyoti Baghel,[1,2] and Sasikumar Elumalai [1, *]

[1] *Chemical Engineering Division, BRIC National Agri-Food and Biomanufacturing Institute (Formerly, Center of Innovative and Applied Bioprocessing), Mohali, Punjab 140306 India*

[2] *Department of Chemical Sciences, Indian Institute of Science Education and Research Mohali (IISER), Mohali, Punjab 140306 India*

*Corresponding author E-mail: sasikumar@ciab.res.in (S. Elumalai); Tel: +91-172-5221-444

[†] Equally contributed authors.

Total Pages: 26

Total Figures: 18

Total Tables: 4

Total Scheme:1

Experimental

Materials

All reagents, solvents, and chemicals used were of analytical grade. Furfural, 2-furoic acid, 2,5-diformylfuran, 2,5-furandicarboxylic acid, silver nitrate solution (2.5% w/v $AgNO_3$ in H_2O), Nafion and D_2O (99.9% atom D) were purchased from Sigma Aldrich (India). Reagent-grade potassium hydroxide (KOH), nitric acid and iodine were procured from SRL chemicals (India). The deionized water (DI) obtained from the Millipore water purifier system (Millipore) was used for sample preparations and dilutions.

Mathematical expressions

$$Product\ yield\ (\%) = \frac{product\ formed\ (mol)}{initial\ substrate\ (mol)} \times 100$$

------- (S1)

$$Product\ selectivity\ (\%) = \frac{product\ yield\ (\%)}{substrate\ conversion\ (\%)} \times 100$$

------- (S2)

$$Substrate\ conversion\ (\%) = \frac{substrate\ reacted\ (mol)}{initial\ substrate\ (mol)} \times 100$$

------- (S3)

Debye-Scherrer's equation:

$$D = \frac{K \times \lambda}{\beta \times Cos\theta}$$

------- (S4)

Where, K is the constant; λ is the incident wavelength of X-ray (1.54056 Å); β is full width at half maxima (FWHM); and θ is the Bragg's angle.

First-order kinetic rate equation

$$ln\left\{\frac{[MO]_t}{[MO]_0}\right\} = -k \times time\ (sec)$$

---------- (S5)

Where, $[MO]_t$ and $[MO]_0$ represent the final and initial reactant (methyl orange dye) concentration at time *t*. *k* is the observed rate constant of MO degradation.

Furfural preparation using corncob

Briefly, 1 g of powdered corncob biomass sample (30 mesh) was mixed with 30 mL of dilute oxalic acid (0.3 M) and 1 mL of dil. H_2SO_4 (0.1 M) in a 100 mL glass reaction tube. The reaction tube was stirred at 400 rpm and heated to the desired temperature (180 °C) for 1 h. After the reaction, the resulting slurry was centrifuged at a high speed (8,000 rpm) to separate the liquid and solid portions. To the liquid fraction, 10 mL dichloromethane (DCM) was added; then, the formed organic layer was separated and evaporated under vacuum conditions to remove DCM. The resulting yellow-coloured liquid was used to determine the concentration of furfural. It was diluted using the Milli-Q water, filtered through a 0.45 µm polytetrafluoroethylene (PTFE) filter membrane and analyzed on a high-performance liquid chromatography (HPLC) equipment (Thermo Fisher 3000 series) equipped with a refractive index (RI) detector, which was maintained at 55 °C. An Agilent Hi-Plex H column (300 mm length and 8 µm porosity) was used for the sample analysis, which was maintained at 65 °C. A 5 mM dilute H_2SO_4 solution was used as a mobile phase at 0.7 ml/min flow.

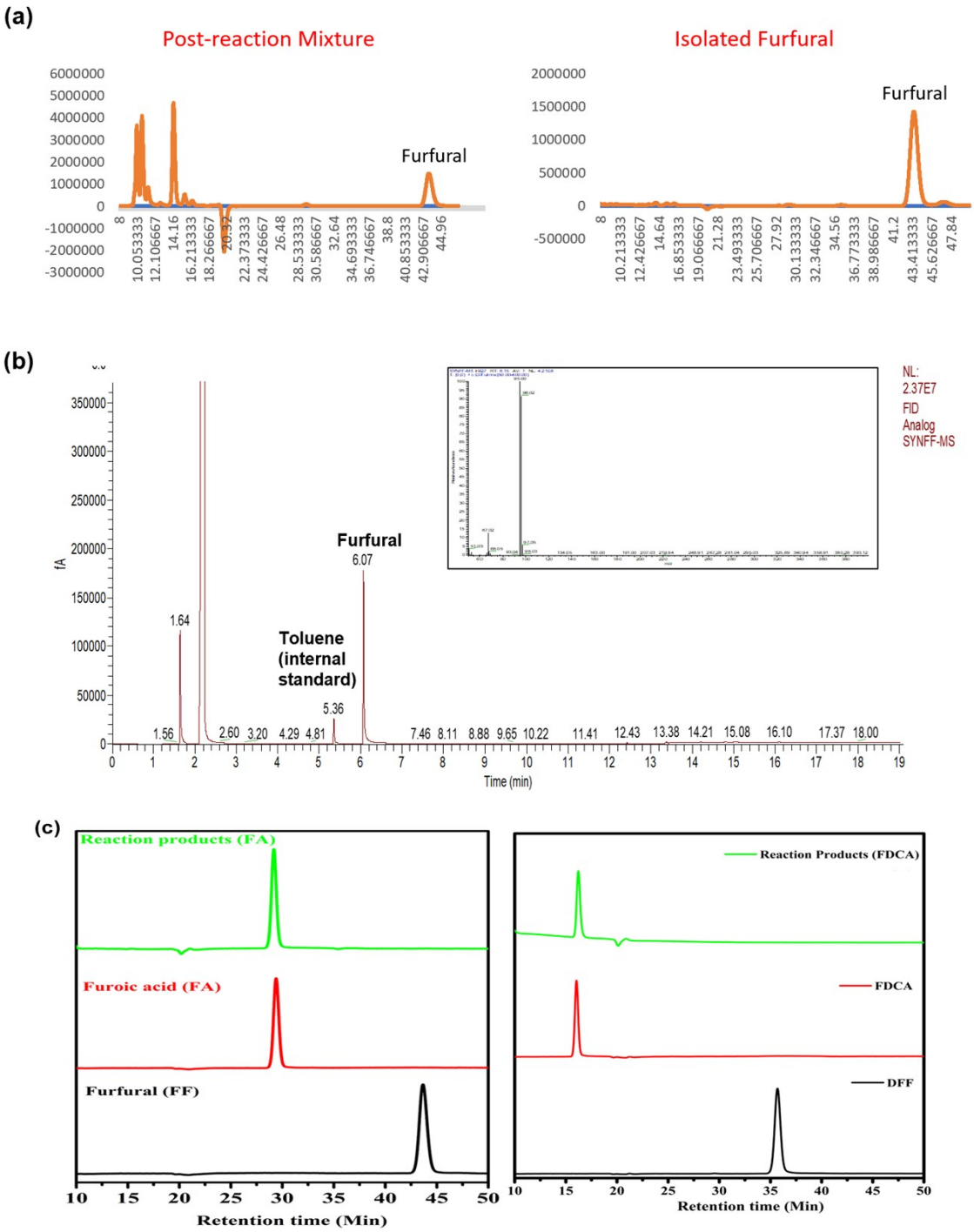

Figure S1. (a) Comparative HPLC chromatogram of post-reaction mixture of corncob digestion using oxalic acid and dilute sulfuric acid and isolation using DCM; (b) GC chromatogram of isolated furfural (inset- GC-MS chromatogram); and, (c) HPLC chromatogram of furfural to FA and DFF to FDCA.

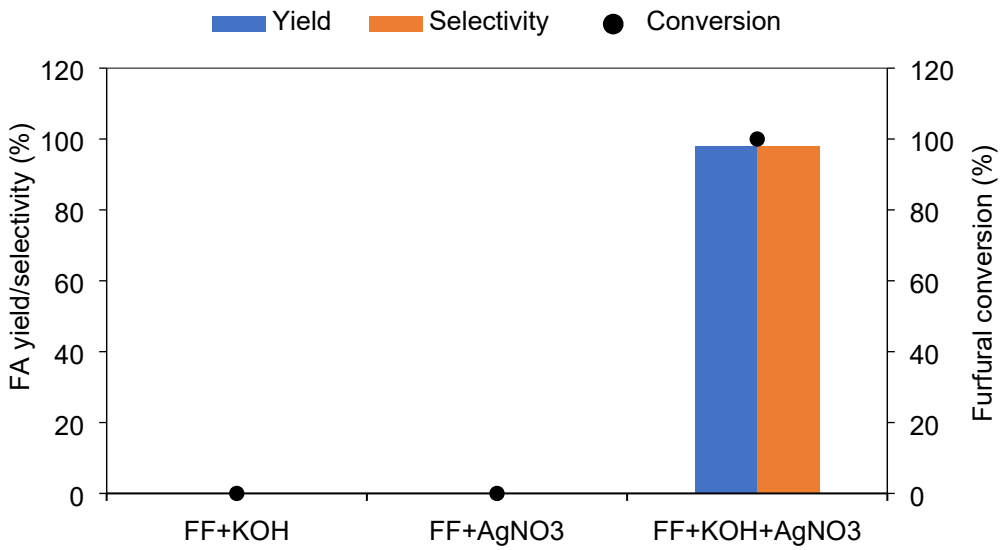

Figure S2. Comparative result of furfural conversion in the presence of either oxidizing ($AgNO_3$) or reducing agent after 1 min under room temperature conditions.

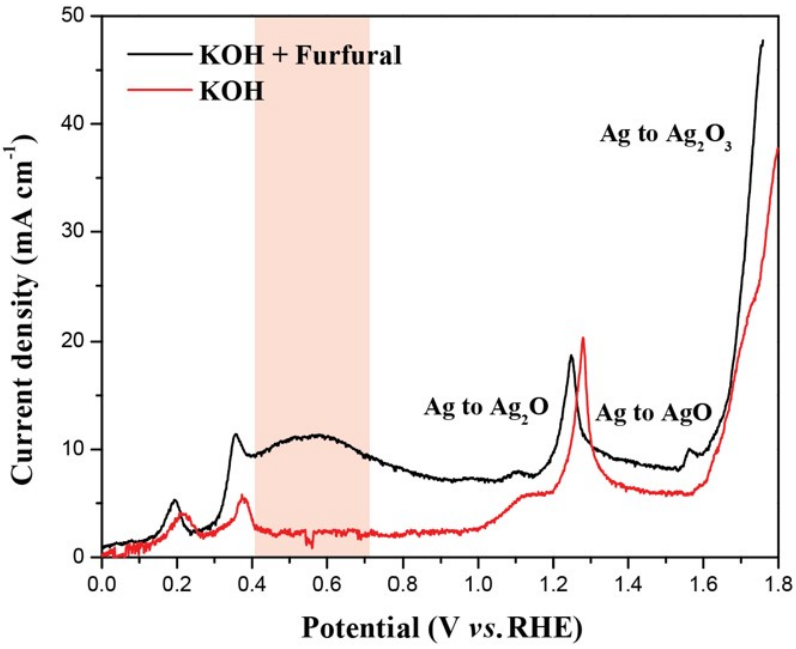

Figure S3. LSV cyclic profile of furfural electrochemical oxidation in a three-electrode system.

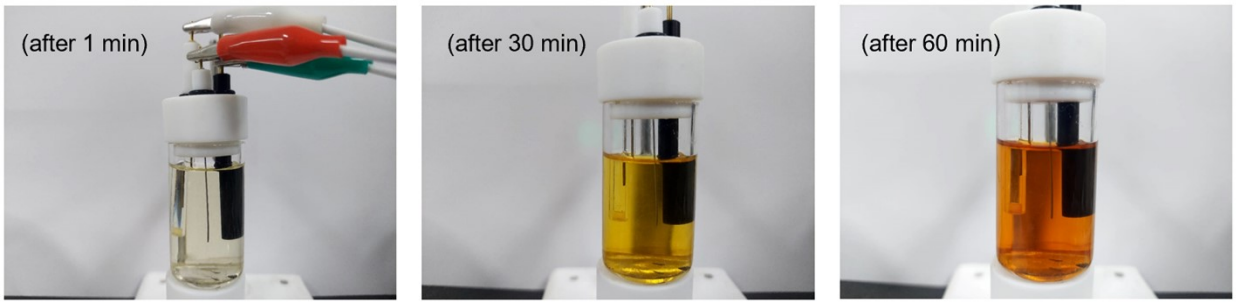

Figure S4. Images of the post-reaction medium of electrooxidation of furfural in a three-electrode system at different time intervals.

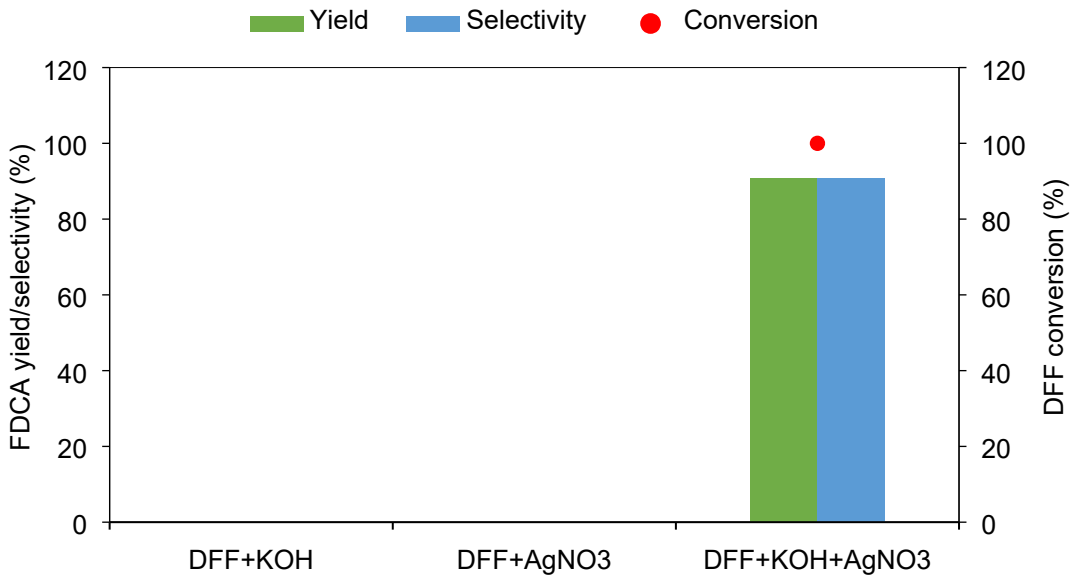

Figure S5. Comparative result of DFF conversion in the presence of either oxidizing ($AgNO_3$) or reducing agent after 1 min under room temperature conditions.

Table S1. Comparative literature data of FA synthesis using furfural to the present work.

Sl. No.	Precursor	Catalyst	Reaction Conditions	Conversion (%)	Yield/ Selectivity (%)	Ref.
1.	Furfural	Ru-Acridine PNP complex	135 °C, 48 h, NaOH	-	95	1
2.	Furfural	MnO_2	100 °C, 1.0 MPa O_2, 12 h	99.04	96.8	2
3.	Furfural	Au-MnO_2	110 °C, 12 bar, air, 4 h	100	82	3
4.	Furfural	Au/ZTC	120 °C, 12 bar, 6 h	89	-	4
5.	Furfural	N-Heterocyclic carbene	DMSO solvent, strong base, 313 K, 4 h, 0.1 MPa O_2	99	57	5
6.	Furfural	AuPd/ $Mg(OH)_2$	P O_2 -3 bar, 303 K	99.5	84.5	6
7.	Furfural	CuO and Ag_2O/CuO	pH 13, 70 °C	-	92	7
8.	Furfural	Au_4Pd_1@SiTi	10 h	99	50	8
9.	Furfural	Au_3Pd_1 catalyst	80 °C	30	100 % selectivity	9
10.	Furfural	Pb/Pt as catalyst, Pt/C as co-catalyst	65 °C, pH 8, 1 h	93	96 % selectivity	10
11.	Furfural	Pt atomic clusters catalyst supported on rehydrated layered double hydroxides (Pt/re-Mg_4Al-LDHs)	60 °C, O_2 pressure 1 MPa, 6 h	99	97	11
12.	Furfural	Ag/TiO_2	25 °C, 15 bar air pressure, NaOH	96	96	12
13.	Furfural	5 wt % Ru/C	Na_2CO_3, 120 °C, 8 h and 10 bar oxygen pressure	96	83	13
14.	Furfural	$AgNO_3$	0.5 M KOH, room temperature	100	>97	This work

Table S2. Comparative literature data of FDCA synthesis using DFF to the present work.

Sl. No.	Precursor	Catalyst	Reaction Conditions	Conversion (%)	Yield/ Selectivity (%)	Ref.
1.	DFF	Combined catalytic system of Co/Mn acetate and N-hydroxyimides in acetic acid	1 mmol substrate, 15 mol% $Co(OAc)_2 \cdot 4H_2O$, 15 mol% $Mn(OAc)_2 \cdot 4H_2O$, 30 mol% NHPI, 110 min.	>99%	98.7	14
2.	DFF	galactose oxidase M3–5, periplas mic aldehyde oxidase (PaoABC), catalase and horseradish peroxidase.	5 mg catalase CLEA, 0.065 mg soluble PaoABC/ 50 mg PaoABC immobilised hydro gel, 0.1 mM KPi pH 7.0, 0.2 M DFF, 37 °C, 1.5 h.	91%	-	15
3.	DFF	$AgNO_3$	0.5 M KOH, room temperature	100	90	This work

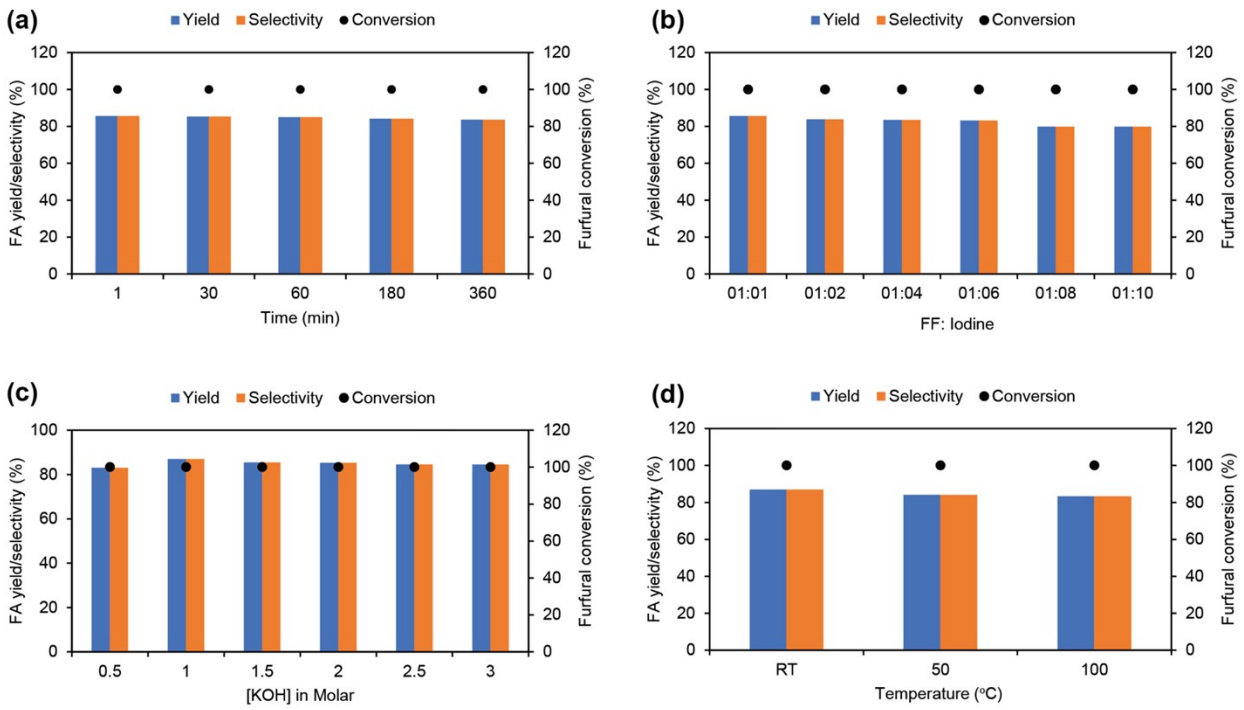

Figure S6. (a) Results of time optimization at room temperature and 1:1 mol ratio DFF to I_2 in KOH medium (0.5 M); (b) I_2 optimization results at room temperature in KOH medium (0.5 M) after 1 min; (c) [KOH] optimization results at room temperature at 1:1 mol ratio DFF to I_2 after 1 min; (d) effect of temperature at 1:1 mol ratio DFF to I_2 in KOH medium (0.5 M) after 1 min; The error bar represents the standard error. The asterisk marks (* and **) denote the mean data significance and non-significance through ANOVA analysis at α=0.05.

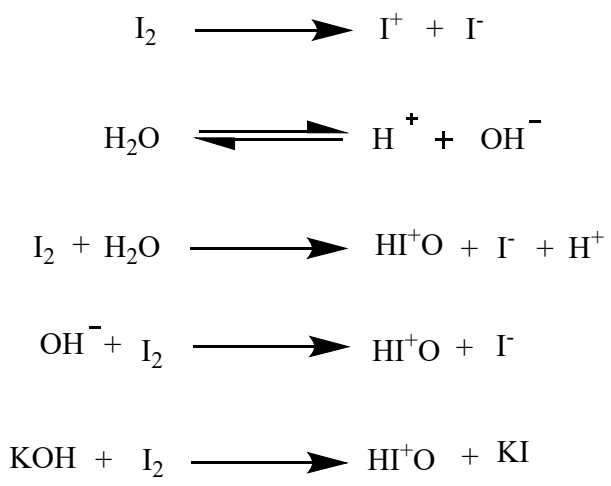

Scheme S1. Proposed reaction scheme of iodine in KOH.

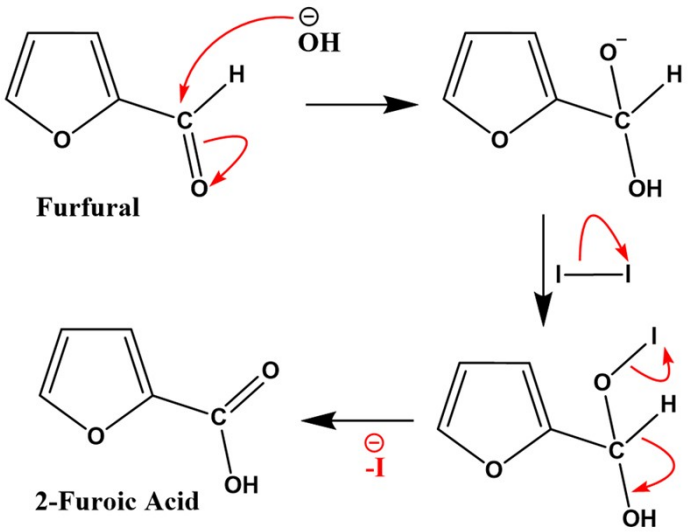

Figure S7. Proposed reaction mechanism of iodine-mediated furfural to FA in an aqueous KOH medium.

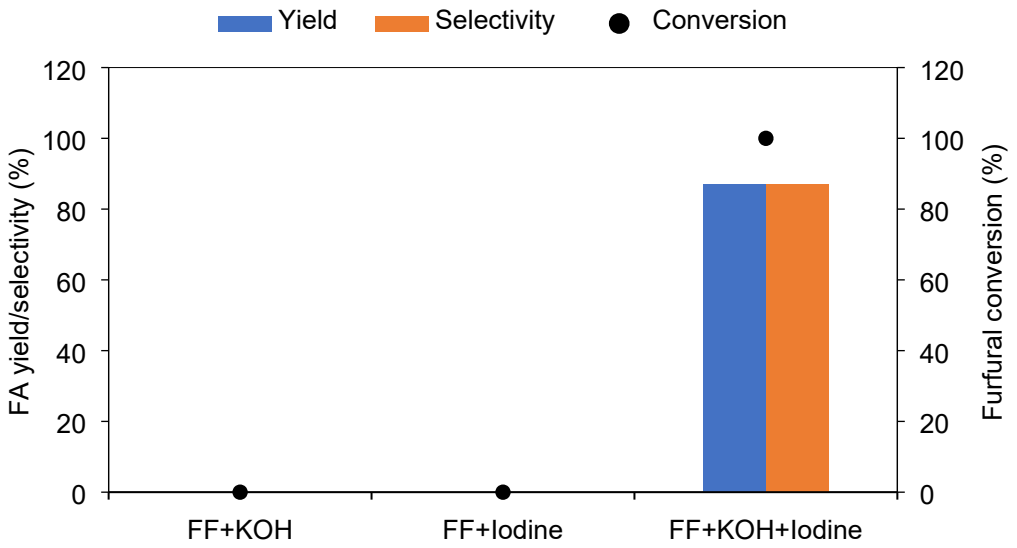

Figure S8. Comparative result of furfural conversion in the presence of either oxidizing (I_2) or reducing agent after 1 min under room temperature conditions.

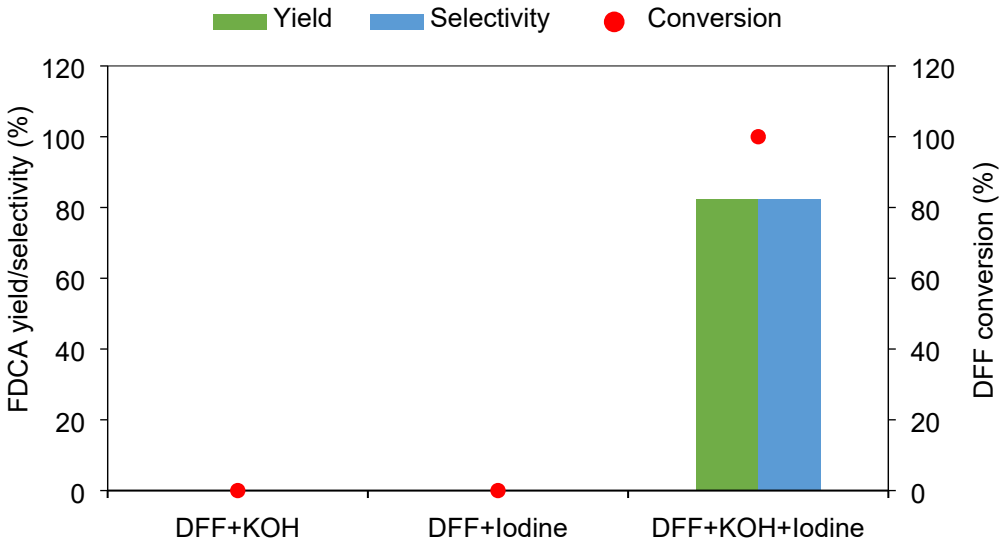

Figure S9. Comparative result of DFF conversion in the presence of either oxidizing (I_2) or reducing agent after 1 min under room temperature conditions.

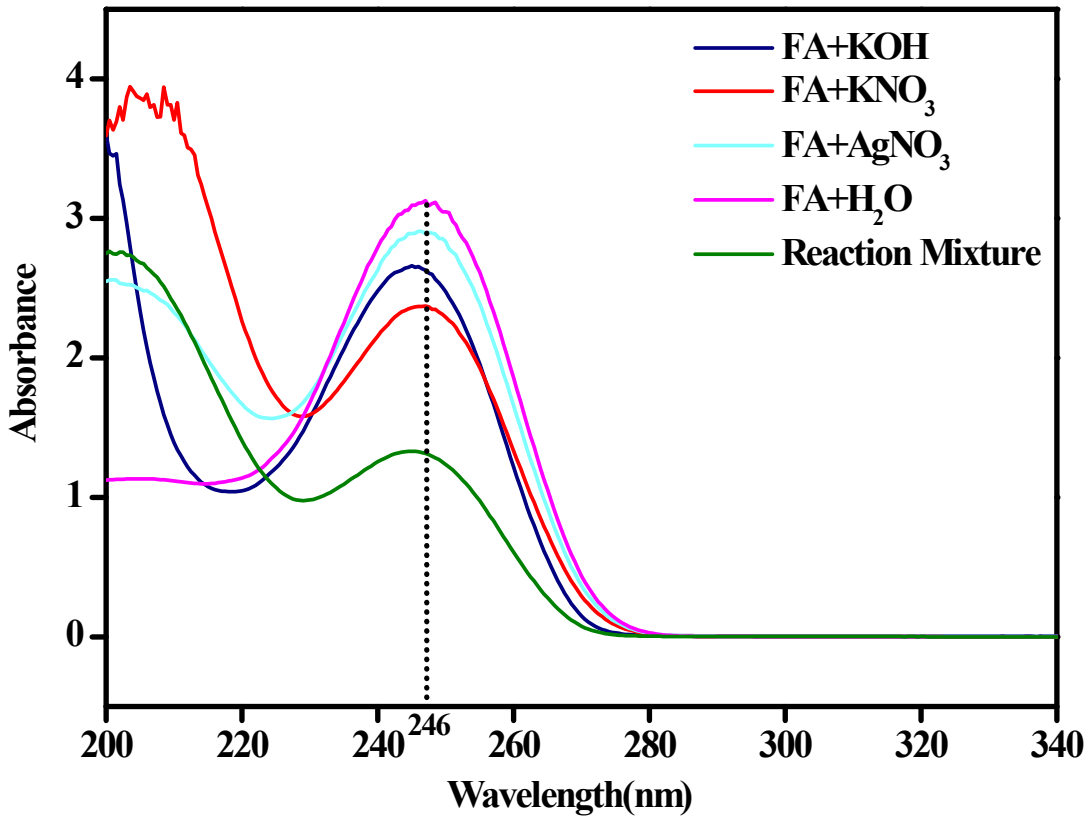

Figure S10. UV-visible spectra of various reaction mixtures: FA (Furoic acid) with KOH, FA with KNO_3, FA with $AgNO_3$, Furoic acid (FA) in water, and reaction mixture.

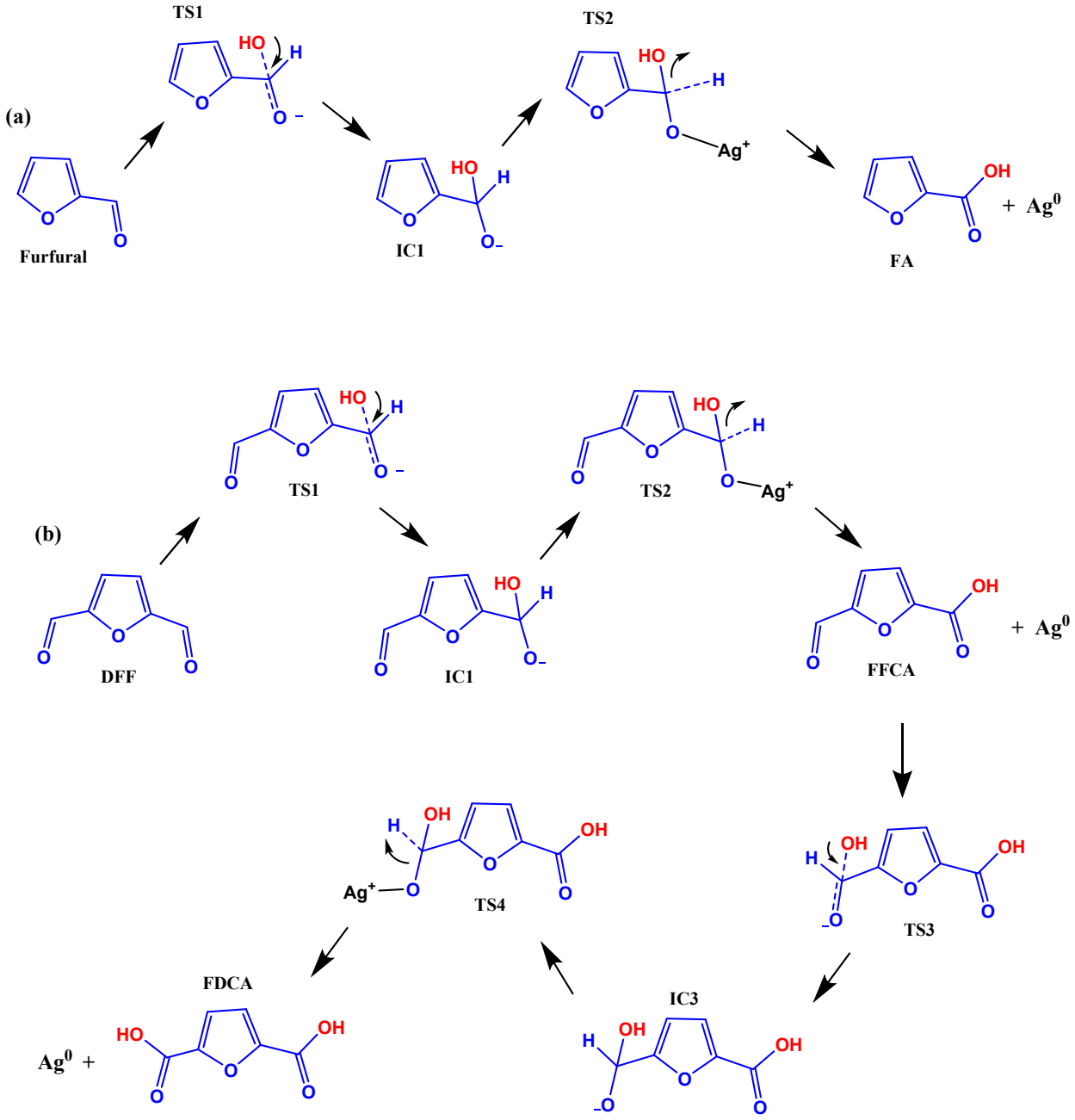

Scheme S1. Proposed reaction schemes of (a) Ag_2O-mediated furfural to FA and (b) DFF to FDCA in an $AgNO_3$-KOH medium.

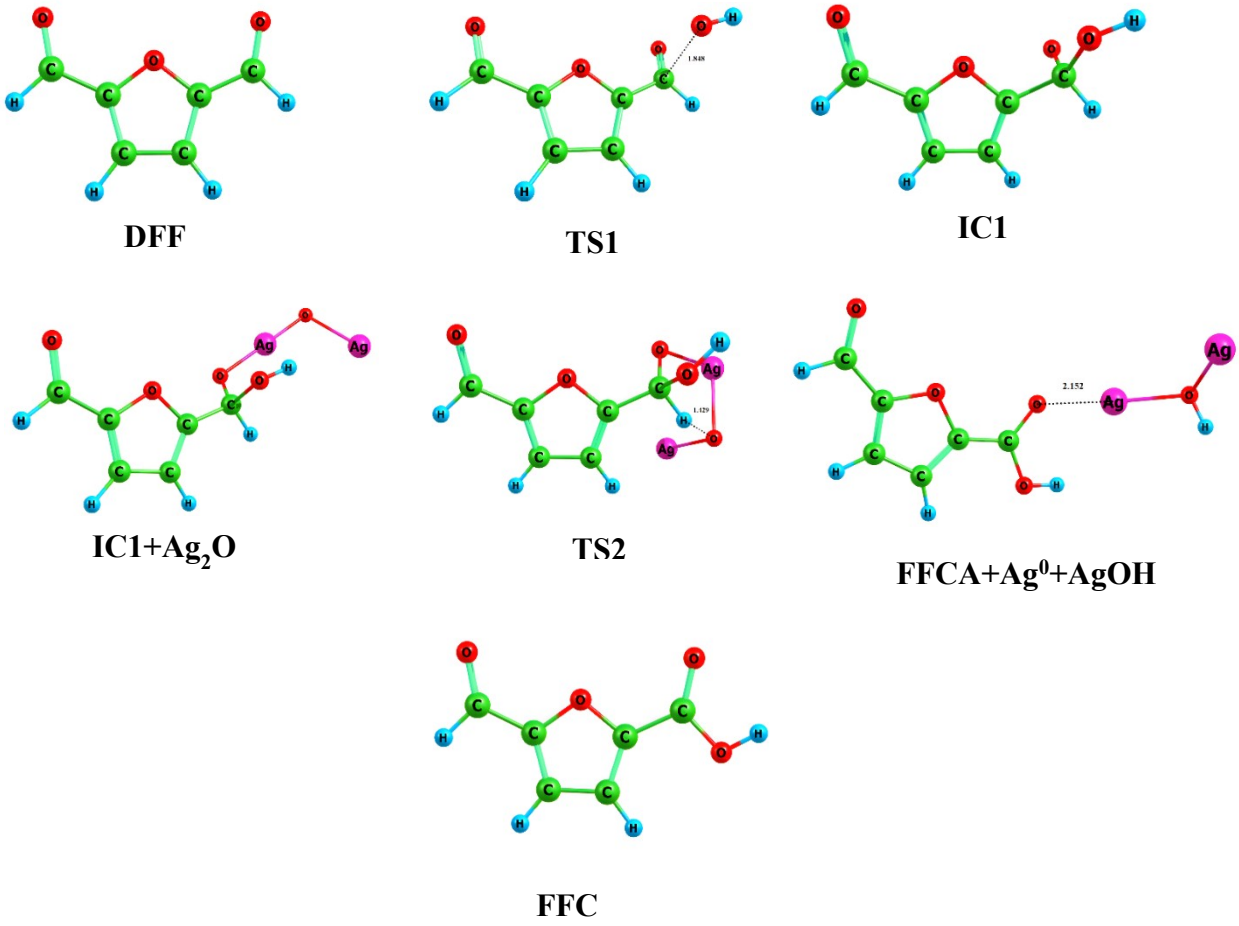

Figure S11. Optimized structures reactant, product, transition state and intermediate molecules involved in the DFF to FFCA via interaction with Ag_2O computed using Gaussian v.16 with the M06 functional and the 6-311++G(d,p)/LANL2DZ basis set.

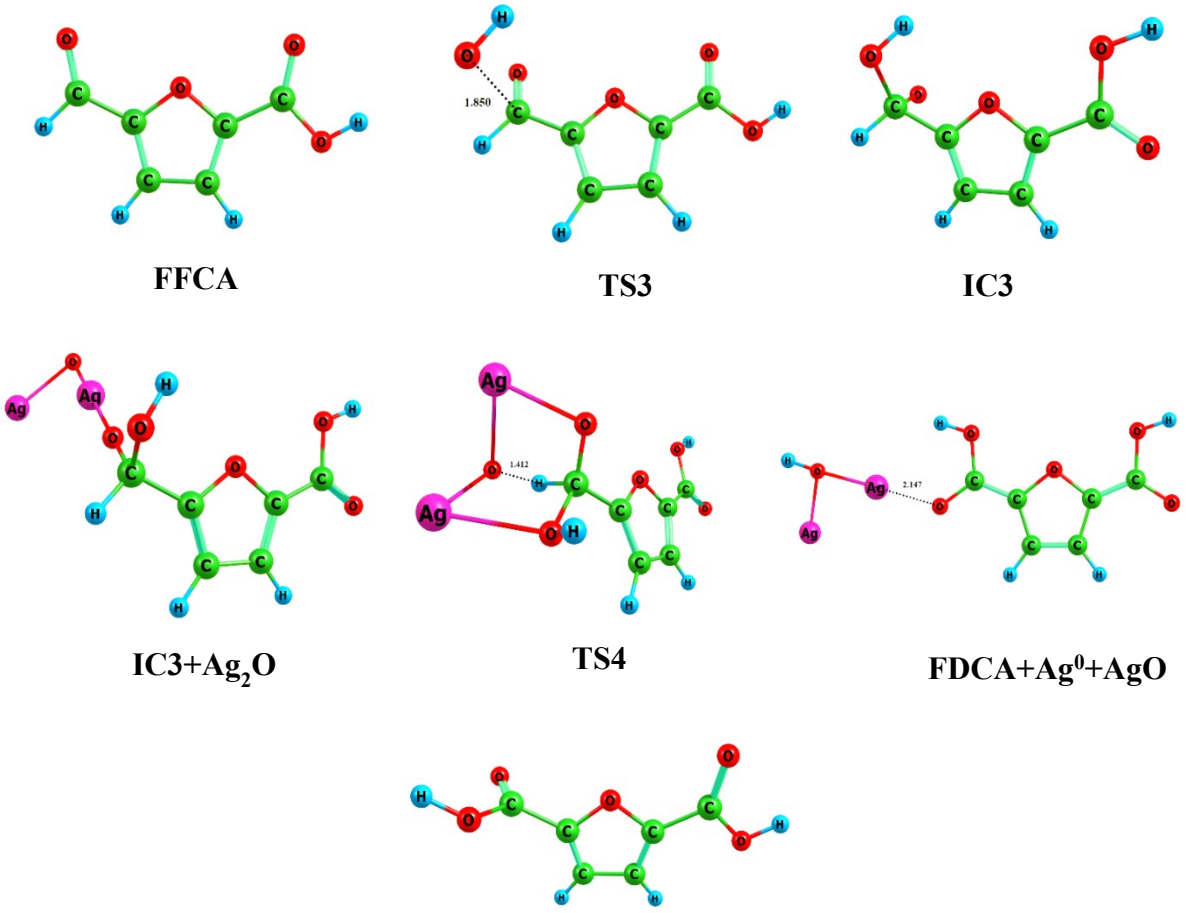

Figure S12. Optimized structures reactant, product, transition state and intermediate molecules involved in the FFCA to FDCA via interaction with Ag_2O computed using Gaussian v.16 with the M06 functional and the 6-311++G(d,p)/LANL2DZ basis set.

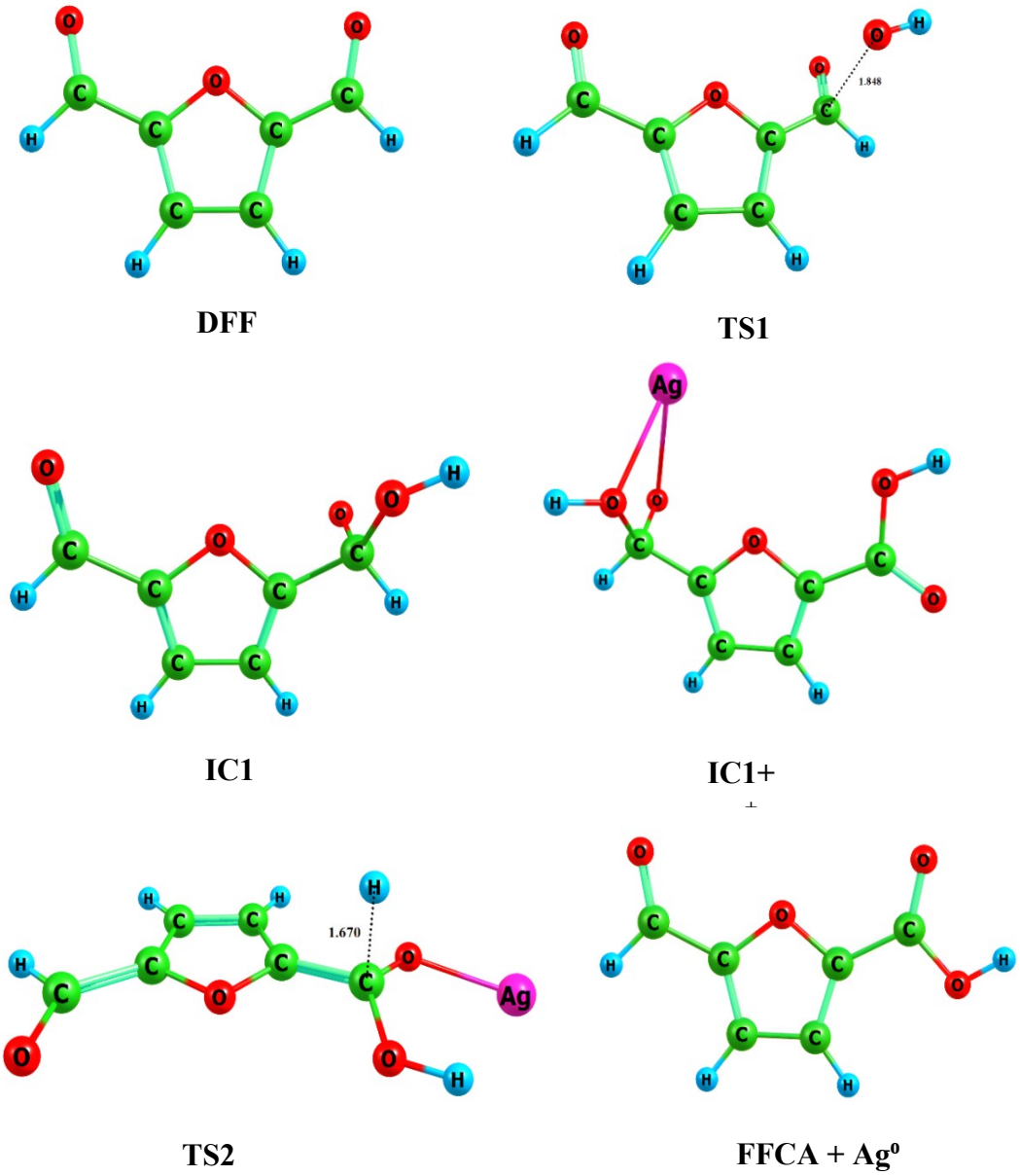

Figure S13. Optimized structures reactant, product, transition state and intermediate molecules involved in the DFF to FFCA via interaction with Ag^{+} computed using Gaussian v.16 with the M06 functional and the 6-311++G(d,p)/LANL2DZ basis set.

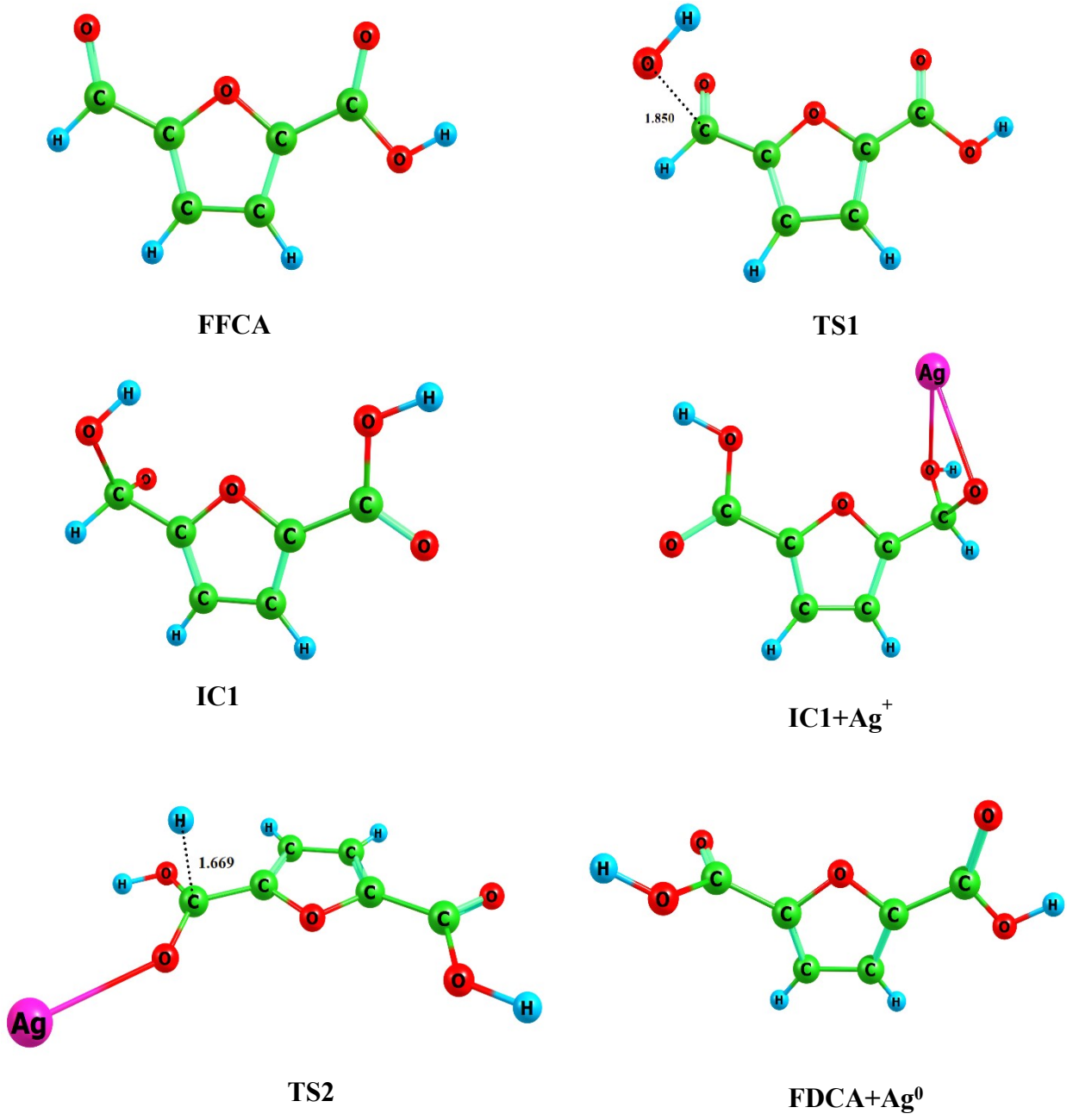

Figure S14. Optimized structures reactant, product, transition state and intermediate molecules involved in the FFCA to FDCA via interaction with Ag^{+} computed using Gaussian v.16 with the M06 functional and the 6-311++G(d,p)/LANL2DZ basis set.

Table S3. Green metrics analysis of FA synthesis

Parameter	Ideal value	Excluding KOH	Including KOH
E-factor	0	0.03	**34.9**
Atom economy (AE)	100	100	100
Carbon Efficiency	100	83.2	83.2
Mass intensity (MI)	1	1.03	35.9
Reaction mass efficiency (RME)	100	96.99	2.79

Table S4. Green metrics analysis of FDCA synthesis

Parameter	Ideal value	Excluding KOH	Including KOH
E-factor	0	0.27	8.16
Atom economy (AE)	100	100	100
Carbon Efficiency	100	89.5	89.5
Mass intensity (MI)	1	1.97	9.16
Reaction mass efficiency (RME)	100	78.7	10.9

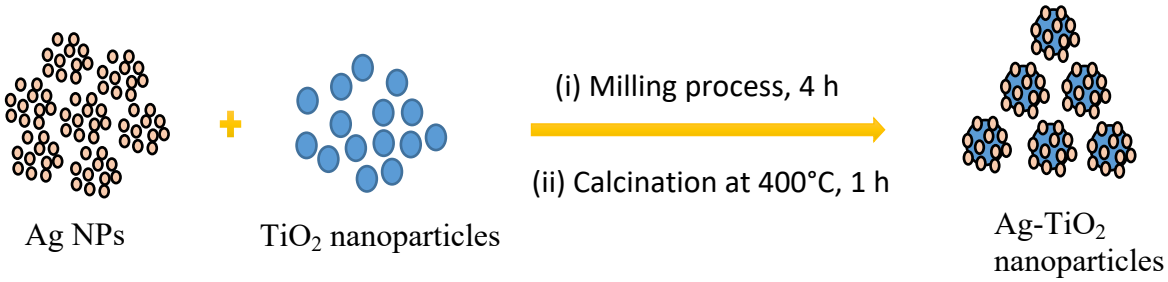

Figure S15. Schematic illustration of Ag-TiO_2 nanocomposite synthesis procedure.

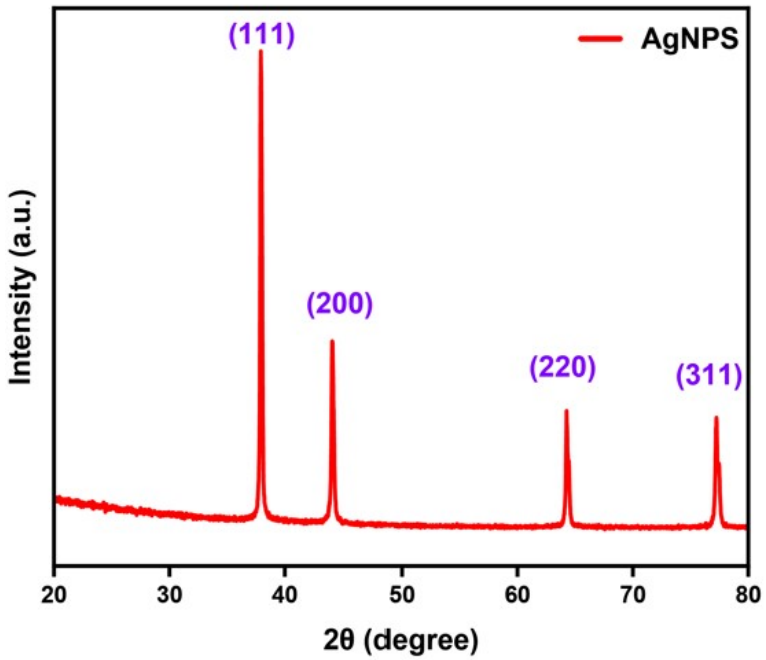

Figure S16. Powder XRD characterization of the recovered Ag NPs from the furfural oxidation in $AgNO_3$-KOH medium after 1 min under optimum conditions.

Discussion: The characteristic XRD pattern can provide information on the atomic arrangement within the nanoparticles, offering insights into their structure and properties. The powder XRD result of Ag NPs is shown in Figure S16; it exhibited sharp and intense peaks at 2θ angles of 38°, 44°, 64° and 77°, corresponding to the (111), (200), (220) and (311) crystallographic planes, assigning a face-centered cubic (FCC) lattice structure of Ag (as per JCPDS card # 04-0783 of Ag crystal). Thus, the results confirm the Ag NPs crystalline characteristics. By employing Debye Scherrer equation (Eqn. S4), the average crystallite size was calculated as 31 nm, consistent with smaller peak widths of larger crystallites. Moreover, the results approve the purity of Ag NPs, based on the absence of additional irrelevant peaks.

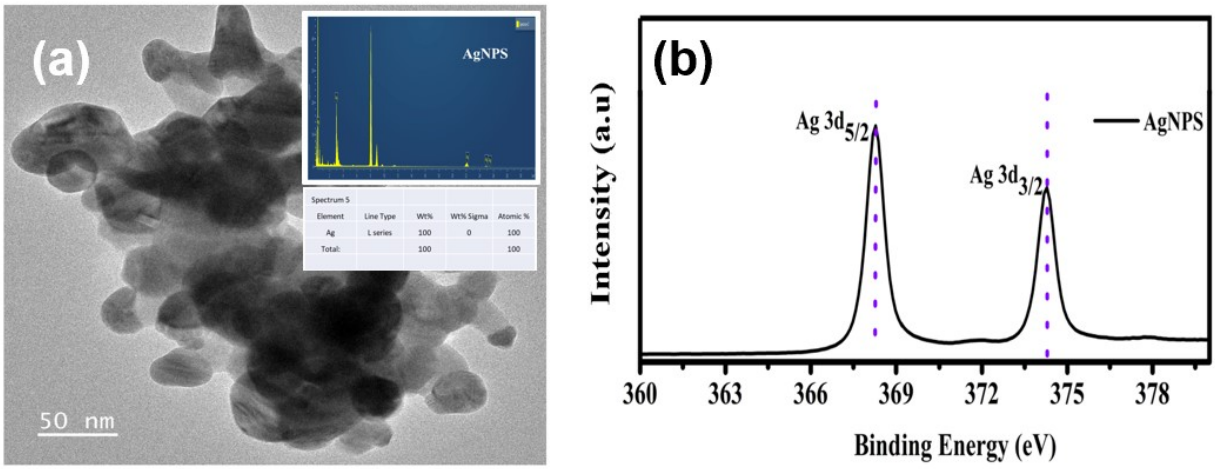

Figure S17. (a) High-resolution TEM image of the recovered Ag NPs, with the inset showing the corresponding EDX spectrum. (b) XPS analysis results depicting the surface chemical composition of the recovered Ag NPs.

Discussion: The topological characteristics of Ag NPs were performed by using HR-TEM; the results display the aggregated spherical form of Ag NPs. The size distribution revealed the average particle sizes as 33 nm (Figure S17a), consistent with the findings of XRD. The EDX analysis further confirmed the maximum synthesis of Ag NPs, as shown in Figure S17a (inset). The determination of chemical environments and oxidation states of synthesized Ag NPs was made using XPS analysis. Figure S17b displays the survey spectrum of Ag $3d_{5/2–3/2}$ (Ag 3d core levels). For Ag NPs, the binding energy was observed to be at 368.1 eV and 374.1 eV, corresponding to Ag $3d_{5/2}$ and Ag $3d_{3/2}$ states, respectively. It is worthwhile that XPS core-level energies are sensitive to a nanoparticle. Therefore, a smaller Ag nanoparticle may exhibit a higher binding energy shift, as reported elsewhere.[16]

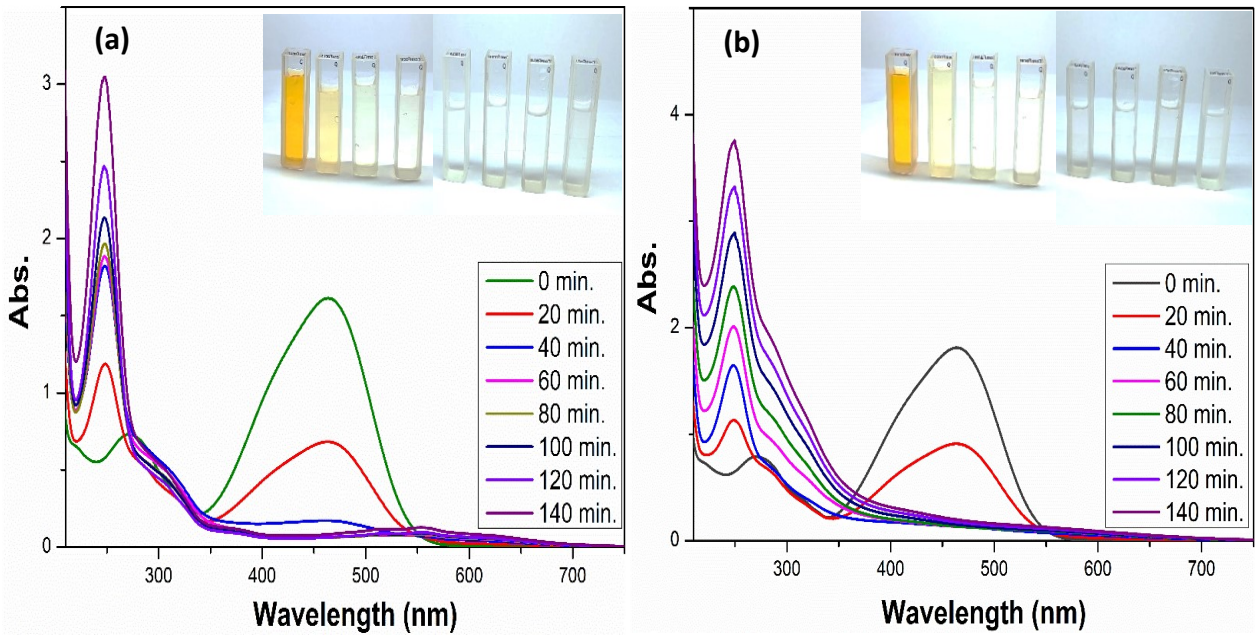

Figure S18. UV-vis absorption spectra of photodegradation of MO under sunlight irradiation over (a) TiO_2 and (b) Ag-TiO_2 under inert conditions (inset: images of MO degradation at different time intervals).

References

(1) Kar, S.; Zhou, Q.-Q.; Ben-David, Y.; Milstein, D. Catalytic Furfural/5-Hydroxymethyl Furfural Oxidation to Furoic Acid/Furan-2,5-dicarboxylic Acid with H2 Production Using Alkaline Water as the Formal Oxidant. *Journal of the American Chemical Society* **2022**, *144* (3), 1288-1295. DOI: 10.1021/jacs.1c10908.

(2) Wu, X.; Guo, H.; Jia, L.; Xiao, Y.; Hou, B.; Li, D. Effect of MnO2 Crystal Type on the Oxidation of Furfural to Furoic Acid. *Catalysts* **2023**, *13* (4), 663.

(3) Ferraz, C. P.; Da Silva, A. G. M.; Rodrigues, T. S.; Camargo, P. H. C.; Paul, S.; Wojcieszak, R. Furfural Oxidation on Gold Supported on MnO2: Influence of the Support Structure on the Catalytic Performances. *Applied Sciences* **2018**, *8* (8), 1246.

(4) Papanikolaou, G.; Lanzafame, P.; Perathoner, S.; Centi, G.; Cozza, D.; Giorgianni, G.; Migliori, M.; Giordano, G. High performance of Au/ZTC based catalysts for the selective oxidation of bio-derivative furfural to 2-furoic acid11This paper in honor of Professor James G. Goodwin, Jr., in the occasion of his 75th birthday, to celebrate his outstanding contribution to catalysis sciences and technology. *Catalysis Communications* **2021**, *149*, 106234. DOI: https://doi.org/10.1016/j.catcom.2020.106234.

(5) Gupta, N. K.; Fukuoka, A.; Nakajima, K. Metal-Free and Selective Oxidation of Furfural to Furoic Acid with an N-Heterocyclic Carbene Catalyst. *ACS Sustainable Chemistry & Engineering* **2018**, *6* (3), 3434-3442. DOI: 10.1021/acssuschemeng.7b03681.

(6) Douthwaite, M.; Huang, X.; Iqbal, S.; Miedziak, P. J.; Brett, G. L.; Kondrat, S. A.; Edwards, J. K.; Sankar, M.; Knight, D. W.; Bethell, D.; et al. The controlled catalytic oxidation of furfural to furoic acid using AuPd/Mg(OH)2. *Catalysis Science & Technology* **2017**, *7* (22), 5284-5293, 10.1039/C7CY01025G. DOI: 10.1039/C7CY01025G.

(7) Tian, Q.; Shi, D.; Sha, Y. CuO and Ag2O/CuO Catalyzed Oxidation of Aldehydes to the Corresponding Carboxylic Acids by Molecular Oxygen. *Molecules* **2008**, *13* (4), 948-957.

(8) P. Ferraz, C.; Costa, N. J. S.; Teixeira-Neto, E.; Teixeira-Neto, Â. A.; Liria, C. W.; Thuriot-Roukos, J.; Machini, M. T.; Froidevaux, R.; Dumeignil, F.; Rossi, L. M.; et al. 5-Hydroxymethylfurfural and Furfural Base-Free Oxidation over AuPd Embedded Bimetallic Nanoparticles. *Catalysts* **2020**, *10* (1), 75.

(9) Al Rawas, H. K.; Ferraz, C. P.; Thuriot-Roukos, J.; Heyte, S.; Paul, S.; Wojcieszak, R. Influence of Pd and Pt Promotion in Gold Based Bimetallic Catalysts on Selectivity Modulation in Furfural Base-Free Oxidation. *Catalysts* **2021**, *11* (10), 1226.

(10) Verdeguer, P.; Merat, N.; Gaset, A. Lead/platinum on charcoal as catalyst for oxidation of furfural. Effect of main parameters. *Applied Catalysis A: General* **1994**, *112* (1), 1-11. DOI: https://doi.org/10.1016/0926-860X(94)80133-9.

(11) Ren, Z.; Yang, Y.; Wang, S.; Li, X.; Feng, H.; Wang, L.; Li, Y.; Zhang, X.; Wei, M. Pt atomic clusters catalysts with local charge transfer towards selective oxidation of furfural. *Applied Catalysis B: Environmental* **2021**, *295*, 120290. DOI: https://doi.org/10.1016/j.apcatb.2021.120290.

(12) Sadier, A.; Paul, S.; Wojcieszak, R. Selective Oxidation of Furfural at Room Temperature on a TiO2-Supported Ag Catalyst. *Catalysts* **2022**, *12* (8), 805.

(13) Lokhande, P.; Dhepe, P. L. Selective and Robust Ru Catalyst for the Aqueous Phase Aerobic Oxidation of Furfural to 2-Furoic Acid. *ACS Applied Materials & Interfaces* **2023**, *15* (40), 47004-47015. DOI: 10.1021/acsami.3c09965.

(14) Xia, F.; Ma, J.; Jia, X.; Guo, M.; Liu, X.; Ma, H.; Gao, J.; Xu, J. Catalytic Synthesis of 2,5-Furandicarboxylic Acid from Concentrated 2,5-Diformylfuran Mediated by N-hydroxyimides under Mild Conditions. *Chemistry – An Asian Journal* **2019**, *14* (19), 3329-3334. DOI: https://doi.org/10.1002/asia.201901001.
(15) McKenna, S. M.; Mines, P.; Law, P.; Kovacs-Schreiner, K.; Birmingham, W. R.; Turner, N. J.; Leimkühler, S.; Carnell, A. J. The continuous oxidation of HMF to FDCA and the immobilisation and stabilisation of periplasmic aldehyde oxidase (PaoABC). *Green Chemistry* **2017**, *19* (19), 4660-4665, 10.1039/C7GC01696D. DOI: 10.1039/C7GC01696D.
(16) Huang, Z.; Jiang, H.; Liu, P.; Sun, J.; Guo, D.; Shan, J.; Gu, N. Continuous synthesis of size-tunable silver nanoparticles by a green electrolysis method and multi-electrode design for high yield. *Journal of Materials Chemistry A* **2015**, *3* (5), 1925-1929, 10.1039/C4TA06782G. DOI: 10.1039/C4TA06782G.